Applied Nonlinear Dynamics and Vibrations
https://www.sciltp.com/journals/andv

Article

Mittag–Leffler Stability and Decay-Rate Enhancement for a Nabla Discrete Fractional-Order Glucose–Insulin Regulatory System with a Nonsingular Mittag–Leffler Kernel

Grienggrai Rajchakit

Program in Industrial Optimisation and Applications, Faculty of Science, Maejo University, Chiang Mai 50290, Thailand; kreangkri@mju.ac.th

How To Cite: Rajchakit, G. Mittag–Leffler Stability and Decay-Rate Enhancement for a Nabla Discrete Fractional-Order Glucose–Insulin Regulatory System with a Nonsingular Mittag–Leffler Kernel. *Applied Nonlinear Dynamics and Vibrations* **2026**, *1*(1), 5.

Received: 22 July 2026
Revised: 2 September 2026
Accepted: 10 September 2026
Published: 18 September 2026

Abstract: We study a reduced-order, discrete-time glucose–insulin regulatory model with an intended nonsingular Mittag–Leffler memory kernel. The aim is an interpretable control-theoretic benchmark, not a patient-specific artificial-pancreas model. For the bidirectionally coupled error system, optimisation of a scalar quadratic Young-inequality estimate gives $\lambda^* = \frac{1}{2}[(a+c) - \sqrt{(a-c)^2 + \beta^2}]$, where $\beta = bL_\phi + eL_\psi$; this algebraic quantity is positive exactly when $\beta < 2\sqrt{ac}$. At $a = 0.6$, $c = 0.4$, and $\beta = 0.5$, it increases the fixed-parameter value from 0.150 to 0.231. Replacing c by $c + k_1$ with $k_1 = 0.6$ gives 0.480. Strict gain monotonicity holds for $\beta > 0$, while the formal $\beta = 0$ extension is nondecreasing and saturates at a. Interpretation of these values as Mittag–Leffler decay certificates remains conditional on the operator definition and comparison lemmas flagged in this proof. The delayed estimate supplies a delay-independent algebraic condition, not a delay-uniform decay rate. The disturbance estimate, if its comparison properties hold, supplies an asymptotic residual radius. An explicit lagged predictor is reproducible and admits an endpoint refinement check, but this check does not establish consistency with the stated operator. In addition, the coupled code omits the equilibrium shifts of the raw model. These operator and model-alignment issues are retained as explicit editorial queries requiring resolution before publication. No clinical performance or safety claim is made.

Keywords: discrete fractional calculus; nabla operator; Mittag–Leffler kernel; glucose–insulin regulation; Mittag–Leffler stability; feedback control

1. Introduction

Diabetes mellitus is a chronic metabolic disorder in which glucose regulation is impaired. Reduced-order GIR models, beginning with the Bergman minimal model [1], are useful because they isolate mechanisms that can be analysed before more detailed physiological or data-driven models are considered. Fractional-order variants add hereditary dependence and have recently been studied with time delays, numerical solvers, fuzzy rules, and feedback control [2–11]. The present model is studied for a narrower reason: it is the smallest nonlinear sampled-data setting in which one can separate (i) a conservative global stability certificate, (ii) the effect of an explicit insulin-feedback gain on that certificate, and (iii) the effects of sensing delay and bounded exogenous inputs. This separation is difficult to see in high-dimensional clinical simulators and is valuable for theory, while remaining insufficient for clinical validation.

Two modelling ingredients are relevant. First, the nonsingular Mittag–Leffler kernel of Atangana and Baleanu [12] has a discrete nabla counterpart [13,14] within discrete fractional calculus [15]. Second, sensing and actuation are sampled, which motivates a discrete rather than continuous state description. Recent Mittag–Leffler analyses span continuous impulsive complex-valued BAM neural networks with time-varying delays [16], nabla discrete-time fuzzy complex-valued molecular networks with boundedness estimates [17], and delayed discrete genetic regulatory networks with finite-time

Copyright: © 2026 by the authors. This is an open access article under the terms and conditions of the Creative Commons Attribution (CC BY) license (https://creativecommons.org/licenses/by/4.0/).
Publisher's Note: Scilight stays neutral with regard to jurisdictional claims in published maps and institutional affiliations.

synchronisation and feedback controllers [18]. These studies establish important Lyapunov, decomposition, and inequality tools, but address network stability, boundedness, or synchronisation rather than decay-certificate tuning for a reduced-order GIR equilibrium. Related nabla stability results [19–21] and delayed summation inequalities [22] provide the mathematical context, while fractional and fuzzy diabetes models continue to develop [23].

The closest predecessor is our earlier nabla discrete ABC GIR study [24], which established existence, uniqueness, Hyers–Ulam stability, and an iterative approximation for an open-loop model. The present contribution is explicitly a refinement and control-oriented extension of that work. The Young-parameter tuning is standard; the contribution claimed here is limited to carrying that free parameter through the coupled GIR Lyapunov estimate, solving the resulting max–min problem in closed form, and extending the certificate to proportional feedback, delayed feedback, and bounded disturbances. Table 1 makes these differences explicit.

Table 1. Comparison with the closest Mittag–Leffler and discrete-fractional studies. "Certificate form" records the principal analytical output rather than a clinical-performance metric.

Study	Model and Objective	Main Technique/Features	Relation to the Present Result
Ali et al. [16]	Continuous fractional complex BAM network; global Mittag–Leffler stability	Lyapunov analysis, complex decomposition, impulses, time-varying delays	Not a GIR model; no feedback-gain to decay-certificate formula.
Narayanan et al. [24]	Nabla discrete ABC GIR; existence and Hyers–Ulam stability	Fixed-point theory and iterative approximation; open loop	Direct predecessor; no decay-certificate optimisation, delayed control, or disturbance radius.
Kchaou et al. [18]	Delayed nabla discrete complex genetic network; finite-time synchronisation	Direct and real-decomposition approaches with linear feedback	Network synchronisation rather than GIR equilibrium regulation.
Narayanan et al. [17]	Nabla discrete fuzzy complex molecular network; global boundedness	Fuzzy rules, Lyapunov inequalities, attraction-set estimates	No GIR interpretation or scalar gain-to-certificate calculation.
Present study	Coupled two-state nabla discrete ABC GIR; global stability	Optimised Young parameter; proportional/delayed feedback; bounded input	Closed-form scalar certificate, optimal only within the stated quadratic estimate.

No artificial neural network is trained or used in this study. A neural-network method would answer a different, data-dependent prediction or control-design question and would require training and test data that are not available here. We therefore compare the proposed analytical certificate with fixed-parameter Lyapunov estimates, fixed-point/iterative analysis, complex decomposition, and fuzzy-network boundedness methods in Table 1; a performance comparison with an artificial neural network would not be methodologically meaningful for the present theorem-driven objective.

Our contributions are as follows.

1. We formulate a fully coupled nabla discrete fractional-order GIR model with bounded, Lipschitz secretion and uptake nonlinearities, prove the existence and uniqueness of a physiological equilibrium for every secretion gain $e \geq 0$, and derive the bidirectionally coupled error dynamics (Section 3).
2. Using a Young-parametrised estimate, we obtain the algebraic condition $\beta < 2\sqrt{ac}$ and the optimal value within that estimate (Theorem 1); its dynamical interpretation is conditional on the operator-specific lemmas flagged below. The choice $\varepsilon = 1$ is recovered in Corollary 1. The bound is sign-agnostic (Remark 1).
3. We analyse a linear insulin-feedback law and show that the certified exponent is strictly increasing in the gain when $\beta > 0$ and converges to the glucose-clearance ceiling a; when $\beta = 0$ it is nondecreasing and reaches a after the insulin mode ceases to be limiting (Theorem 2).
4. Conditional on the operator-specific comparison and Halanay properties identified below, we derive a delay-magnitude-independent criterion for delayed insulin feedback (Proposition 2) and an asymptotic residual-set bound under bounded meal disturbances (Corollary 2).
5. The explicit-predictor computations, endpoint refinement check, and parameter studies are reported in Section 5. Their consistency with the stated ABC operator remains unresolved; they do not constitute patient validation.

The analysis uses the proposed discrete fractional comparison and quadratic inequalities; it invokes neither an unproved fractional chain rule nor a restart of the memory history. The distinction between fractional operators matters when applying existing stability results [19], and the operator-specific prerequisites are flagged below.

2. Preliminaries

We collect the discrete fractional calculus needed below; see [14,15] for details. For $a \in \mathbb{R}$ write $\mathbb{N}_a = \{a, a+1, a+2, \dots\}$, and let $\nabla x(t) = x(t) - x(t-1)$ denote the backward (nabla) difference.

Definition 1 (Nabla fractional sum and Caputo difference [15])**.** *For $x : \mathbb{N}_a \to \mathbb{R}$ and $\alpha > 0$, the α-th nabla fractional sum is*

$$ {}_a\nabla^{-\alpha} x(t) = \frac{1}{\Gamma(\alpha)} \sum_{s=a+1}^{t} \big(t - \rho(s)\big)^{\overline{\alpha-1}} x(s), \qquad t \in \mathbb{N}_{a+1}, \tag{1} $$

where $\rho(s) = s - 1$ and $t^{\overline{\alpha}} = \Gamma(t+\alpha)/\Gamma(t)$ is the rising factorial. For $0 < \alpha < 1$, the nabla Caputo fractional difference is

$$ {}^{C}\nabla^{\alpha} x(t) = {}_a\nabla^{-(1-\alpha)} \nabla x(t) = \frac{1}{\Gamma(1-\alpha)} \sum_{s=a+1}^{t} \big(t - \rho(s)\big)^{\overline{-\alpha}} \nabla x(s). \tag{2} $$

For the model we use the Atangana–Baleanu–Caputo (ABC) nabla difference [13,14]

$$ {}^{ABC}\nabla^{\alpha} x(t) = \frac{M(\alpha)}{1-\alpha} \sum_{s=a+1}^{t} \nabla x(s)\, \mathcal{E}_{\overline{\alpha}}\left(-\frac{\alpha}{1-\alpha}, t - \rho(s) \right), \tag{3} $$

where $M(0) = M(1) = 1$ and, additionally, $M(\alpha) > 0$ on the working range. Its associated fractional sum is

$$ {}^{AB}\nabla^{-\alpha} f(t) = \frac{1-\alpha}{M(\alpha)} f(t) + \frac{\alpha}{M(\alpha)}\, {}_a\nabla^{-\alpha} f(t). \tag{4} $$

The stability results below use the ABC comparison, quadratic, and Halanay inequalities stated in Lemmas 1–4. Keeping the operator explicit in every inequality removes ambiguity between the ordinary Caputo nabla and ABC nabla notation.

Definition 2 (Discrete Mittag–Leffler function [14,19])**.** *For $\lambda \in \mathbb{R}$, $|\lambda| < 1$, and $\alpha, \beta > 0$, the nabla discrete Mittag–Leffler function is $\mathcal{E}_{\overline{\alpha,\beta}}(\lambda, t) = \sum_{k=0}^{\infty} \lambda^k \dfrac{t^{\overline{\alpha k + \beta - 1}}}{\Gamma(\alpha k + \beta)}$, and we write $\mathcal{E}_{\alpha}(\lambda, t) = \mathcal{E}_{\overline{\alpha,1}}(\lambda, t)$.*

Lemma 1 (ABC-nabla comparison principle [13,25])**.** *Let $v, w : \mathbb{N}_a \to \mathbb{R}$ satisfy ${}^{ABC}\nabla^{\alpha} v(t) \le -\lambda v(t) + \mu$ and ${}^{ABC}\nabla^{\alpha} w(t) = -\lambda w(t) + \mu$ with $v(a) \le w(a)$ and $\lambda > 0$ in the stability region of the operator. Then $v(t) \le w(t)$ for all $t \in \mathbb{N}_a$, and w is the corresponding ABC discrete Mittag–Leffler response, denoted below by $\mathcal{E}_{\alpha}^{AB}$.*

Lemma 2 (ABC-nabla quadratic inequality [13,26])**.** *For any $x : \mathbb{N}_a \to \mathbb{R}$ and $0 < \alpha < 1$,*

$$ {}^{ABC}\nabla^{\alpha}\big(x^2(t)\big) \;\le\; 2\, x(t)\, {}^{ABC}\nabla^{\alpha} x(t), \qquad t \in \mathbb{N}_{a+1}. \tag{5} $$

Lemma 3 (Discrete Mittag–Leffler stability [19])**.** *Let $V : \mathbb{N}_a \to [0, \infty)$ satisfy ${}^{ABC}\nabla^{\alpha} V(t) \le -\lambda V(t)$ with $\lambda > 0$ in the stability region of the ABC nabla operator. Then $V(t) \le V(a)\, \mathcal{E}_{\alpha}^{AB}(-\lambda, t - a)$ and $V(t) \to 0$ as $t \to \infty$.*

Lemma 4 (Discrete fractional Halanay inequality [26])**.** *Let $V \ge 0$ satisfy ${}^{ABC}\nabla^{\alpha} V(t) \le -p\, V(t) + q \max_{t-\tau \le s \le t} V(s)$ for $t \in \mathbb{N}_{a+1}$, with constants $p > q > 0$ and $\tau \in \mathbb{N}_0$. Then there exists $\lambda^{\sharp} \in (0, p - q]$ such that $V(t) \le M\, \mathcal{E}_{\alpha}^{AB}(-\lambda^{\sharp}, t - a)$, where $M = \max_{a-\tau \le s \le a} V(s)$; in particular $V(t) \to 0$ regardless of the magnitude of τ.*

We shall repeatedly use the parametrised Young inequality: for all $x, y \in \mathbb{R}$ and every $\varepsilon > 0$,

$$ |x|\,|y| \;\le\; \frac{\varepsilon}{2}\, x^2 + \frac{1}{2\varepsilon}\, y^2. \tag{6} $$

3. Model Formulation

3.1. The Nabla Discrete Fractional GIR System

Let $G(t)$ and $I(t)$ denote, respectively, the plasma glucose concentration and the interstitial insulin action at the sampling instant $t \in \mathbb{N}_0$, expressed relative to fasting reference levels. We consider the nabla discrete fractional-order GIR model

$$
{}^{ABC}\nabla^{\alpha} G(t) = -a\,G(t) - b\,\phi\big(I(t)\big) + p, \tag{7}
$$

$$
{}^{ABC}\nabla^{\alpha} I(t) = -c\,I(t) + e\,\psi\big(G(t)\big) + u(t), \tag{8}
$$

for $t \in \mathbb{N}_1$, with fractional order $\alpha \in (0,1)$. Here $a > 0$ is the insulin-independent glucose clearance rate, $c > 0$ the insulin decay rate, $b > 0$ the maximal insulin-mediated glucose-uptake gain, $e \geq 0$ the glucose-stimulated insulin-secretion gain, $p > 0$ the constant hepatic glucose production, and $u(t)$ an abstract deviation in insulin delivery about a basal value. The functions $\phi, \psi : \mathbb{R} \to \mathbb{R}$ represent saturating uptake and secretion characteristics.

Assumption 1. *ϕ and ψ are continuous, monotone nondecreasing, with $\phi(0) = \psi(0) = 0$, and globally Lipschitz with constants $L_\phi, L_\psi > 0$; moreover ϕ and ψ are bounded, $|\phi(x)| \leq \bar{\phi}$, $|\psi(x)| \leq \bar{\psi}$. A representative choice is $\phi(x) = \psi(x) = \tanh(x)$, for which $L_\phi = L_\psi = 1$ and $\bar{\phi} = \bar{\psi} = 1$.*

Scope and Dimensional Interpretation

The two states are scaled deviations rather than directly measured glucose and insulin concentrations, and the coefficients used below are illustrative dimensionless quantities. The model omits meal-absorption compartments, subcutaneous insulin pharmacokinetics, sensor noise, actuator saturation, hypoglycaemia constraints, inter-patient variability, and parameter estimation from clinical records. Consequently, $u = -k_1 i$ is a mathematical feedback benchmark and not a deployable dosing law. The analysis asks how a feedback coefficient changes a provable stability margin under stated Lipschitz bounds; it does not claim to predict patient glucose or validate an artificial-pancreas controller.

Proposition 1 (Physiological equilibrium)**.** *Under Assumption 1, for every secretion gain $e \geq 0$ the uncontrolled systems (7) and (8) ($u \equiv 0$) admit a unique equilibrium (G^*, I^*) with $I^* = (e/c)\,\psi(G^*)$ and G^* the unique positive root of*

$$
H(G) := a\,G + b\,\phi\Big(\tfrac{e}{c}\psi(G)\Big) - p = 0. \tag{9}
$$

Proof. At equilibrium ${}^{ABC}\nabla^{\alpha} G = {}^{ABC}\nabla^{\alpha} I = 0$. The second equation gives $cI^* = e\psi(G^*)$, i.e., $I^* = (e/c)\psi(G^*)$; substituting into the first yields $H(G^*) = 0$. The map H is continuous and, by Assumption 1 (with $a > 0$ and ϕ, ψ nondecreasing), strictly increasing; moreover $H(0) = b\phi(0) - p = -p < 0$ and $H(G) \to +\infty$ as $G \to +\infty$. By the intermediate value theorem and strict monotonicity, Equation (9) has a unique root $G^* > 0$. For $e = 0$ this reduces to $I^* = 0$, $G^* = p/a$. □

3.2. Error Dynamics

Introduce the regulation error $g(t) = G(t) - G^*$, $i(t) = I(t) - I^*$, and the shifted nonlinearities $\tilde{\phi}(i) = \phi(i + I^*) - \phi(I^*)$ and $\tilde{\psi}(g) = \psi(g + G^*) - \psi(G^*)$, which satisfy $\tilde{\phi}(0) = \tilde{\psi}(0) = 0$ and, by Assumption 1, $|\tilde{\phi}(i)| \leq L_\phi |i|$, $|\tilde{\psi}(g)| \leq L_\psi |g|$. Since ${}^{ABC}\nabla^{\alpha}$ annihilates constants, Equations (7) and (8) become the bidirectionally coupled error system

$$
{}^{ABC}\nabla^{\alpha} g(t) = -a\,g(t) - b\,\tilde{\phi}\big(i(t)\big), \tag{10}
$$

$$
{}^{ABC}\nabla^{\alpha} i(t) = -c\,i(t) + e\,\tilde{\psi}\big(g(t)\big) + u(t). \tag{11}
$$

Regulation of glucose to the physiological level G^* is thus equivalent to stabilisation of the origin of Equations (10) and (11). Write $e(t) = (g(t), i(t))^\top$. The glucose-to-insulin secretion term $e\,\tilde{\psi}(g)$ is the physiological cross-coupling absent from the decoupled ($e = 0$) analysis of [24]; together with the insulin-to-glucose uptake term it closes a negative-feedback loop (Remark 1).

4. Main Results

4.1. Optimised Open-Loop Mittag–Leffler Certificate

The following theorem retains the free parameter ε in the Young inequality (6). The resulting value is optimal only within the stated scalar quadratic Lyapunov estimate and the magnitude bound in (17); it is not asserted to be the true optimal decay rate of the nonlinear fractional system.

Theorem 1 (Optimised quadratic Mittag–Leffler certificate)**.** *Assume a well-defined ABC operator for which Lemmas 2 and 3 hold at the decay parameter used below, as required by M01–M02. Let Assumption 1 hold, let $u \equiv 0$, and set the combined coupling gain*

$$\beta := bL_\phi + eL_\psi. \tag{12}$$

If

$$\beta \; < \; 2\sqrt{ac}, \tag{13}$$

then the origin of Equations (10) and (11) is globally discrete Mittag–Leffler stable, and

$$\|e(t)\|_2^2 \; \le \; \|e(0)\|_2^2 \, \mathcal{E}_\alpha^{AB}\big(-2\lambda^*,\, t\big), \tag{14}$$

with the least-conservative guaranteed exponent within this Lyapunov/Young estimate,

$$\lambda^* \; = \; \tfrac{1}{2}\Big[(a+c) - \sqrt{(a-c)^2+\beta^2}\Big] \; > \; 0. \tag{15}$$

Proof. Take $V(t) = \frac{1}{2}\big(g^2(t) + i^2(t)\big) \ge 0$. By Lemma 2 applied to each component and summed,

$${}^{ABC}\nabla^\alpha V(t) \le g(t)\, {}^{ABC}\nabla^\alpha g(t) + i(t)\, {}^{ABC}\nabla^\alpha i(t). \tag{16}$$

Substituting (10) and (11) with $u \equiv 0$ and using $|\tilde{\phi}(i)| \le L_\phi |i|$, $|\tilde{\psi}(g)| \le L_\psi |g|$ (Assumption 1),

$$\begin{aligned} {}^{ABC}\nabla^\alpha V(t) &\le -a\, g^2 - b\, g\, \tilde{\phi}(i) - c\, i^2 + e\, i\, \tilde{\psi}(g) \\ &\le -a\, g^2 + \big(bL_\phi + eL_\psi\big)|g||i| - c\, i^2 = -a\, g^2 + \beta |g||i| - c\, i^2. \end{aligned} \tag{17}$$

The two coupling terms—insulin-mediated uptake (bL_ϕ) and glucose-stimulated secretion (eL_ψ)—enter the estimate only through their sum β. Apply (6) with an arbitrary parameter $\varepsilon > 0$ to the cross term, $\beta|g||i| \le \frac{\beta\varepsilon}{2} g^2 + \frac{\beta}{2\varepsilon} i^2$, giving

$${}^{ABC}\nabla^\alpha V(t) \le -A(\varepsilon)\, g^2 - C(\varepsilon)\, i^2, \qquad A(\varepsilon) = a - \tfrac{\beta\varepsilon}{2}, \;\; C(\varepsilon) = c - \tfrac{\beta}{2\varepsilon}. \tag{18}$$

Consequently ${}^{ABC}\nabla^\alpha V(t) \le -2\lambda(\varepsilon) V(t)$ with $\lambda(\varepsilon) = \min\{A(\varepsilon), C(\varepsilon)\}$. If $\beta > 0$, A is strictly decreasing and C strictly increasing in ε, so the best certificate within this one-parameter estimate is obtained where the two coincide, $A(\varepsilon^*) = C(\varepsilon^*)$, i.e.,

$$a - \tfrac{\beta\varepsilon^*}{2} = c - \tfrac{\beta}{2\varepsilon^*} \implies \beta\,(\varepsilon^*)^2 + 2(c-a)\varepsilon^* - \beta = 0, \tag{19}$$

whose positive root is $\varepsilon^* = \big[(a-c) + \sqrt{(a-c)^2+\beta^2}\big]/\beta$. Substituting back,

$$\lambda^* = A(\varepsilon^*) = a - \tfrac{\beta\varepsilon^*}{2} = \tfrac{1}{2}\Big[(a+c) - \sqrt{(a-c)^2+\beta^2}\Big], \tag{20}$$

which is (15). Positivity of λ^* is equivalent to $(a+c) > \sqrt{(a-c)^2+\beta^2}$; squaring (both sides positive) gives $(a+c)^2 > (a-c)^2 + \beta^2$, i.e., $4ac > \beta^2$, which is exactly (13). With $\lambda^* > 0$, Lemma 3 gives (14). If $\beta = 0$, the cross term vanishes and the same conclusion follows directly with $\lambda^* = \min\{a, c\}$; no division by β or finite optimiser ε^* is then required. □

Corollary 1 (Recovery of the classical and decoupled criteria)**.** *The choice $\varepsilon = 1$ in (18) gives the customary sufficient condition $\min\{a,c\} > \frac{1}{2}\beta$ and exponent $\lambda_0 = \min\{a,c\} - \frac{1}{2}\beta$. Since $\sqrt{ac} \ge \min\{a,c\}$, condition (13) is no stronger, and $\lambda^* \ge \lambda_0$ with equality iff $a = c$ or $\beta = 0$. The decoupled model of [24] is the case $e = 0$, i.e., $\beta = bL_\phi$.*

Proof. Setting $\varepsilon = 1$ in (18) gives $A(1) = a - \frac{1}{2}\beta$, $C(1) = c - \frac{1}{2}\beta$, hence $\lambda(1) = \min\{a,c\} - \frac{1}{2}\beta = \lambda_0$; positivity is $\min\{a, c\} > \frac{1}{2}\beta$, i.e., $\beta < 2\min\{a, c\} \le 2\sqrt{ac}$. The inequality $\lambda^* \ge \lambda_0$ holds because $\lambda^* = \max_{\varepsilon>0} \lambda(\varepsilon) \ge \lambda(1) = \lambda_0$. For $\beta > 0$, the strictly decreasing A and strictly increasing C have a unique intersection and a unique max–min optimiser. Equality therefore forces $\varepsilon^* = 1$, equivalent to $a = c$; conversely $a = c$ gives this optimiser. For $\beta = 0$, both estimates equal $\min\{a, c\}$ for every $a, c > 0$ and every $\varepsilon > 0$. This last case is the formal uncoupled extension; with the stated $b, L_\phi > 0$, the model itself has $\beta > 0$. □

Remark 1 (Robust guarantee versus the true sign structure)**.** *The estimate* (17) *bounds both couplings by $|g||i|$, so it discards their signs. The gains add into $\beta = bL_\phi + eL_\psi$, and the candidate guaranteed exponent decreases as e grows, vanishing at $\beta = 2\sqrt{ac}$. If ϕ and ψ are differentiable at the equilibrium, the actual Jacobian is*

$$J = \begin{pmatrix} -a & -b\phi'(I^*) \\ e\psi'(G^*) & -(c + k_1) \end{pmatrix}.$$

Monotonicity gives nonnegative derivatives, so $\operatorname{tr} J = -a - c - k_1 < 0$ *and* $\det J = a(c + k_1) + be\phi'(I^*)\psi'(G^*) > 0$*. Thus J is Hurwitz as an ordinary differential-equation matrix. For $\phi = \psi = \tanh$, the derivatives are* $\operatorname{sech}^2(I^*)$ *and* $\operatorname{sech}^2(G^*)$*, not generally one. This sign calculation does not by itself establish stability for the ABC difference operator, whose spectral criterion still needs justification. The scalar bound is therefore not an actual decay-rate measurement or evidence that secretion harms regulation.*

Remark 2. *The Young optimisation is exact and costs nothing analytically. Away from the balanced case its benefit is significant: for $a = 0.6$, $c = 0.4$, $\beta = 0.5$ one finds $\lambda_0 = 0.150$ but $\lambda^* = 0.231$, a 54% larger guaranteed exponent; for $a = 0.9$, $c = 0.3$, $\beta = 0.4$ the gap is $\lambda_0 = 0.100$ versus $\lambda^* = 0.239$.*

4.2. Decay-Rate Enhancement by Insulin Feedback

We now activate the actuator with the proportional insulin-feedback law

$$u(t) = -k_1\, i(t), \qquad k_1 \ge 0, \tag{21}$$

which augments the physiological insulin decay. The closed loop is (10) together with ${}^{ABC}\nabla^\alpha i = -(c+k_1)i + e\,\tilde{\psi}(g)$.

Theorem 2 (Monotone decay-rate enhancement)**.** *Under the same operator-specific prerequisites as Theorem 1, now at the closed-loop decay parameter, let Assumption 1 and* (13) *hold, and apply* (21)*. Then the closed-loop origin is globally discrete Mittag–Leffler stable with guaranteed exponent*

$$\lambda^*(k_1) = \tfrac{1}{2}\Big[(a + c + k_1) - \sqrt{(a - c - k_1)^2 + \beta^2}\Big], \qquad \beta = bL_\phi + eL_\psi. \tag{22}$$

If $\beta > 0$, the map $k_1 \mapsto \lambda^*(k_1)$ is strictly increasing on $[0, \infty)$ and approaches a from below as $k_1 \to \infty$. If $\beta = 0$, then $\lambda^*(k_1) = \min\{a, c + k_1\}$: it increases only while $c + k_1 < a$ and is constant thereafter. Thus strict improvement for every positive gain and an unattainable ceiling are asserted only for $\beta > 0$.

Proof. The control $u = -k_1 i$ contributes $-k_1 i^2 \le 0$ to $i\,{}^{ABC}\nabla^\alpha i$, so the derivation of Theorem 1 applies with c replaced by $c + k_1$; (22) follows from (15). Write $\delta = c + k_1$. For $\beta > 0$, $\lambda^* = \frac{1}{2}[(a + \delta) - \sqrt{(a - \delta)^2 + \beta^2}]$ and

$$\frac{d\lambda^*}{d\delta} = \tfrac{1}{2}\Big[1 - \frac{\delta - a}{\sqrt{(a - \delta)^2 + \beta^2}}\Big] > 0, \tag{23}$$

because $\sqrt{(a - \delta)^2 + \beta^2} > |\delta - a| \ge \delta - a$ for $\beta > 0$. Hence λ^* is strictly increasing in δ, and therefore in k_1. As $\delta \to \infty$,

$$\lambda^* = \tfrac{1}{2}\Big[(a + \delta) - (\delta - a)\sqrt{1 + \tfrac{\beta^2}{(\delta - a)^2}}\Big] = a - \frac{\beta^2}{4(\delta - a)} + O(\delta^{-2}) \uparrow a, \tag{24}$$

so a is approached from below and never attained. For $\beta = 0$, (22) reduces directly to $\frac{1}{2}[(a+\delta) - |a - \delta|] = \min\{a, \delta\}$, which proves the stated nondecreasing, eventually constant behaviour. □

Remark 3. *For $\beta > 0$, the optimised certificate* (22) *rises smoothly with diminishing returns of order $1/k_1$, unlike the conventional $\varepsilon = 1$ certificate, which is constant for $k_1 \ge \max\{0, a - c\}$. This is a transparent analytical gain-to-certificate relation. It is not a dosing rule: actuator limits, safety constraints, patient variability, and trajectory-level performance are outside the model.*

4.3. Delayed Feedback and Disturbance Rejection

In sampled implementations the insulin-action measurement reaches the controller after a sensing delay $\tau \in \mathbb{N}_0$, giving $u(t) = -k_1 i(t-\tau)$. The next result is delay-magnitude-independent: only boundedness of τ is required.

Proposition 2 (Delay-independent stability)**.** *Conditional on valid instances of Lemmas 2 and 4 for the specified operator, let Assumption 1 hold and let $u(t) = -k_1 i(t-\tau)$ with $k_1 > 0$, $\tau \in \mathbb{N}_0$. If there exists $\varepsilon > 0$ such that*

$$2\min\Big\{a - \tfrac{\beta\varepsilon}{2},\ c - \tfrac{\beta}{2\varepsilon} - \tfrac{k_1}{2}\Big\} \ > \ k_1, \tag{25}$$

then the closed-loop origin is globally discrete Mittag–Leffler stable, for every τ.

Proof. With $V = \frac{1}{2}(g^2 + i^2)$, Lemma 2 and the substitution of the delayed control give

$${}^{ABC}\nabla^{\alpha} V(t) \le -ag^2 + \beta|g||i| - ci^2 - k_1\, i(t)\, i(t-\tau). \tag{26}$$

Bounding the cross terms by (6) (parameter ε for $|g||i|$, parameter 1 for $|i(t)||i(t-\tau)|$),

$${}^{ABC}\nabla^{\alpha} V(t) \le -A(\varepsilon)g^2 - \big(C(\varepsilon) - \tfrac{k_1}{2}\big)i^2 + \tfrac{k_1}{2} i^2(t-\tau), \tag{27}$$

with A, C from (18). Using $g^2 + i^2 = 2V$ and $i^2(t-\tau) \le 2V(t-\tau)$,

$${}^{ABC}\nabla^{\alpha} V(t) \le -p\, V(t) + q \max_{t-\tau \le s \le t} V(s), \quad p = 2\min\{A(\varepsilon), C(\varepsilon) - \tfrac{k_1}{2}\},\ q = k_1. \tag{28}$$

Condition (25) states $p > q$. Subject to a valid operator-specific Lemma 4, it gives Mittag–Leffler decay for each fixed finite τ, with a decay parameter that may depend on τ. The algebraic condition is independent of the delay magnitude; no uniform positive decay rate over all delays is established. □

Remark 4. *Optimising ε in (25) can enlarge the admissible gain window. The delayed term is bounded by a history maximum, not by the current state alone. If the required Halanay lemma is established, the condition applies to each finite delay at the cost of a gain restriction; the decay parameter may deteriorate as the delay increases.*

Corollary 2 (Practical stability under bounded meal disturbance)**.** *Conditional on the quadratic inequality and the forced comparison formula in the proof below, let a bounded meal input $w(t)$ with $|w(t)| \le \bar{w}$ be added to (10), and let Assumption 1 and (13) hold under (21). With $\lambda^* = \lambda^*(k_1)$ from (22), every such trajectory satisfies*

$$\|e(t)\|_2^2 \le \|e(0)\|_2^2\, \mathcal{E}_{\alpha}^{AB}(-\lambda^*, t) + \frac{\bar{w}^2}{(\lambda^*)^2}\Big[1 - \mathcal{E}_{\alpha}^{AB}(-\lambda^*, t)\Big], \tag{29}$$

provided the normalized comparison response has $r(0) = 1$, $0 \le r(t) \le 1$, and $r(t) \to 0$, where $r(t) = \mathcal{E}_{\alpha}^{AB}(-\lambda^*, t)$. Consequently, $\limsup_{t\to\infty} \|e(t)\|_2 \le R := \bar{w}/\lambda^*$, and every ball of radius $R + \eta$, $\eta > 0$, is eventually entered and retained. Finite-time entry into the exact closed ball of radius R is not implied. This ball is invariant under the displayed bound for initial errors already inside it. For $\bar{w} = 0$ the estimate yields convergence to zero, but not the sharper decay parameter $2\lambda^*$ of Theorem 2.

Proof. Carrying the disturbance through the proof of Theorem 2 adds $g\,w$ to ${}^{ABC}\nabla^{\alpha} V$. By (6) with parameter λ^*, $g\,w \le \frac{\lambda^*}{2} g^2 + \frac{1}{2\lambda^*}\bar{w}^2$. Absorbing $\frac{\lambda^*}{2} g^2$ into the (at least $2\lambda^*$-strong) negative quadratic form leaves ${}^{ABC}\nabla^{\alpha} V(t) \le -\lambda^* V(t) + \frac{1}{2\lambda^*}\bar{w}^2$. By the comparison principle Lemma 1 with $\mu = \bar{w}^2/(2\lambda^*)$, $V(t) \le V(0)\mathcal{E}_{\alpha}^{AB}(-\lambda^*, t) + \frac{\mu}{\lambda^*}[1 - \mathcal{E}_{\alpha}^{AB}(-\lambda^*, t)]$; using $V = \frac{1}{2}\|e\|_2^2$ and $\mu/\lambda^* = \bar{w}^2/(2(\lambda^*)^2)$ gives (29). Set $E_0 = \|e(0)\|_2^2$ and $R = \bar{w}/\lambda^*$. The right-hand side is $R^2 + (E_0 - R^2)r(t)$. Its limit is R^2, proving the limsup claim. For $\eta > 0$, the positive gap $(R+\eta)^2 - R^2$ eventually exceeds $\max\{E_0 - R^2, 0\} r(t)$, which proves eventual retention in the larger ball. If $E_0 \le R^2$, positivity of r gives the invariant bound R^2 at every time. If $E_0 > R^2$ and $r(t) > 0$ at finite times, the comparison bound remains strictly above R^2 and cannot certify exact-ball entry. These implications use the response properties explicitly stated above; their applicability to the manuscript's operator remains query M02. □

5. Numerical Simulations

We evaluate the following explicit predictor, motivated by the local term and memory sum in (4):

$$x_n = x_0 + \frac{1-\alpha}{M(\alpha)} F(t_n, x_{n-1}) + \frac{\alpha h^\alpha}{M(\alpha)} \sum_{k=1}^{n} w_k F(t_{n-k+1}, x_{n-k}), \qquad (30)$$
$$w_k = \frac{\Gamma(k+\alpha-1)}{\Gamma(k)\Gamma(\alpha)}.$$

The one-step lag makes the update explicit and distinguishes it from a current-state implicit sum equation. Local Lipschitz continuity alone does not imply that this replacement has $O(h)$ error. For example, if $F(x) = -\kappa x$ and $x_0 = 1$, the first increment is $-\kappa[1-\alpha+\alpha h^\alpha]/M(\alpha)$, which has a nonzero limit as $h \to 0$. As $\alpha \to 1$ and $M(\alpha) \to 1$, the local term vanishes, $w_k \to 1$, and subtraction of consecutive updates yields the formal forward-Euler limit $x_n - x_{n-1} = hF(t_n, x_{n-1})$. This limiting identity is not a convergence theorem for the ABC equation.

For (30) with $\alpha = 0.9$, $F(x) = -0.5x$, and $x_0 = 1$, Table 2 reports endpoints at $T = 20$ and observed orders computed from unrounded values by

$$p_h = \log_2\left(\frac{|x_h(20) - x_{h/2}(20)|}{|x_{h/2}(20) - x_{h/4}(20)|}\right).$$

The values 0.861, 0.929, and 0.965 are an empirical endpoint self-refinement diagnostic, not validation of the stated ABC model or a proof of first-order convergence.

Table 2. Endpoint refinement test for the explicit predictor (30). Each observed order uses three successive meshes; dashes indicate that the required finer mesh was not computed.

h	1	1/2	1/4	1/8	1/16
$x_h(20)$	0.018905	0.019736	0.020193	0.020433	0.020556
p_h	0.861	0.929	0.965	—	—

For the explicit-predictor illustration we use $M(\alpha) = 1 - \alpha + \alpha/\Gamma(\alpha)$, zero-centred error nonlinearities $\tanh(i)$ and $\tanh(g)$, $a = 0.6$, $b = 0.5$, $c = 0.4$, $\alpha = 0.95$, and $(g_0, i_0) = (8, -3)$. These values are dimensionless and illustrative. In the decoupled benchmark $e = 0$, $\beta = 0.5 < 2\sqrt{ac} \approx 0.980$; the algebraic formula (15) gives $\lambda^*(0) = 0.231$, versus $\lambda_0 = 0.150$ for $\varepsilon = 1$.

5.1. Open Versus Closed Loop

Figure 1 compares predictor trajectories at $k_1 = 0$ and $k_1 = 0.6$. The algebraic values are $\lambda^*(0) = 0.231$ and $\lambda^*(0.6) = 0.480$. For this initial condition, the closed-loop predictor first enters $\|e\|_2 \le 0.1$ at $n = 13$, compared with $n = 19$ in open loop, and its terminal error at $n = 140$ is 7.93×10^{-3} versus 1.04×10^{-2}.

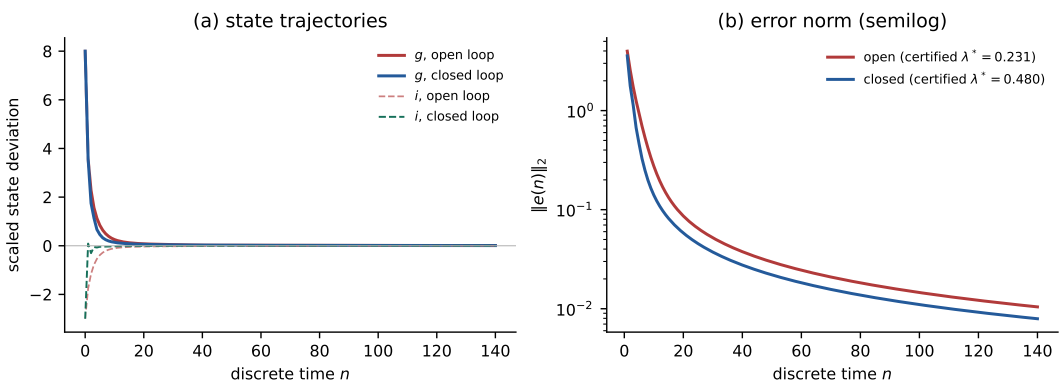

Figure 1. Open-loop versus closed-loop explicit-predictor benchmark. The retained legend's "certified" values 0.231 and 0.480 are algebraic outputs of (22), not fitted trajectory rates; their operator-level certification remains subject to M01–M03.

5.2. *Effect of the Fractional Order*

Figure 2 shows the closed-loop predictor error for $\alpha \in \{0.85, 0.90, 0.95, 0.99\}$. The computed $\|e(120)\|_2$ decreases from 4.98×10^{-2} to 1.45×10^{-3} over this range. This is a parameter sweep of the supplied recurrence, not a validation of the kernel definition, an asymptotic tail law, or physiological performance.

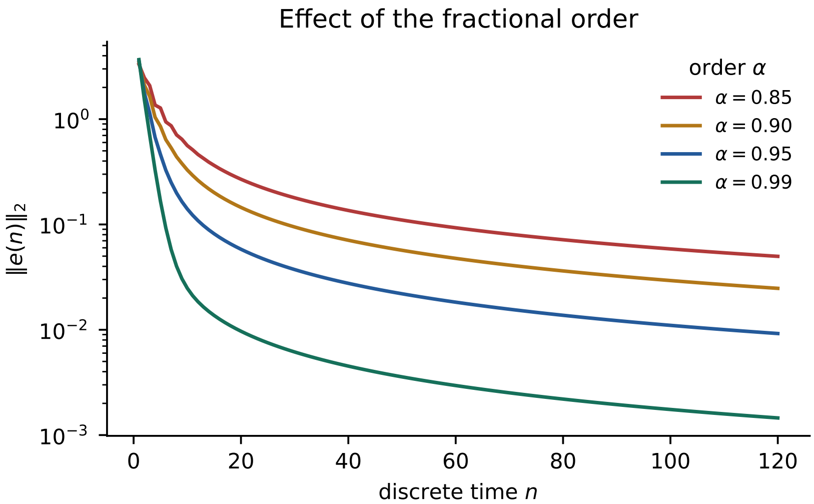

Figure 2. Closed-loop predictor error for four order parameters. The displayed finite-horizon computations do not establish a Mittag–Leffler tail for the manuscript's operator; see M01 and M03.

5.3. *Comparison with the Fixed-Parameter Estimate*

Table 3 compares the conventional choice $\varepsilon = 1$, $\lambda_0(k_1) = \min\{a, c + k_1\} - \frac{1}{2}bL_\phi$, with the optimised Young-parameter certificate. The former saturates at 0.350 for $k_1 \geq 0.2$, whereas the latter equals 0.480 at $k_1 = 0.6$ and approaches $a = 0.6$ when $\beta > 0$. This is a comparison of two analytical certificates, not a claim of system-wide optimal control.

Table 3. Fixed-parameter certificate λ_0 versus the optimised Young-parameter certificate λ^* ($a = 0.6$, $c = 0.4$, $\beta = 0.5$).

k_1	0	0.1	0.2	0.6	1.2	3.0
$\lambda_0(k_1)$	0.150	0.250	0.350	0.350	0.350	0.350
$\lambda^*(k_1)$	0.231	0.295	0.350	0.480	0.541	0.578

5.4. *Coupled Model: Certificate Versus One Trajectory Metric*

For the zero-centred coupled predictor, $\beta = 0.5 + e$. The exact algebraic boundary is $e < 2\sqrt{0.6 \cdot 0.4} - 0.5 = 0.479795897\ldots$, not the rounded strict inequality $e < 0.48$. In Table 4, the open-loop algebraic value decreases toward zero at this boundary, while the predictor's terminal error decreases from 1.04×10^{-2} to 5.27×10^{-3}. Figure 3 displays those open-loop predictor trajectories. These finite-horizon observations do not resolve the raw-model mismatch in M04 or establish a globally optimal trajectory rate.

Table 4. Coupled predictor illustration ($\beta = 0.5 + e$, algebraic boundary $e < 2\sqrt{ac} - 0.5$). The λ^* columns are values of (22), subject to M01–M02; $\|e(140)\|_2$ is a predictor metric, subject to M03–M04.

e	β	$\lambda^*(0)$	$\lambda^*(0.6)$	$\|e(140)\|_2$
0.00	0.50	0.231	0.480	1.04×10^{-2}
0.30	0.80	0.088	0.353	5.93×10^{-3}
0.45	0.95	0.015	0.285	5.27×10^{-3}

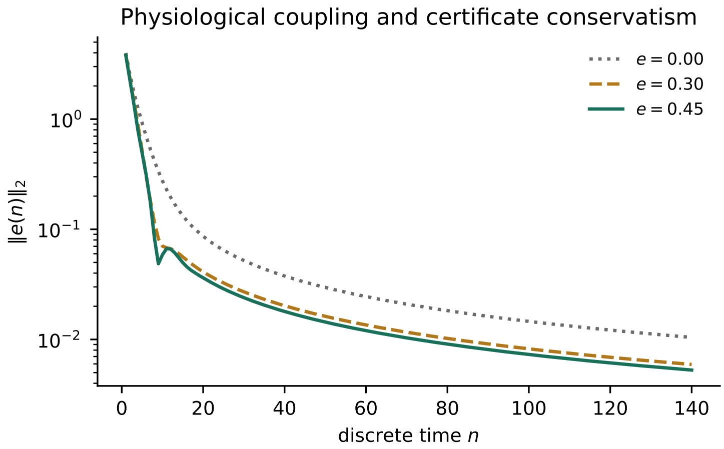

Figure 3. Open-loop predictor error norms for $e = 0$, 0.30, and 0.45. The retained plot title does not establish physiological validity: the code uses zero-centred nonlinearities, and the operator and equilibrium-shift queries M01–M04 remain open.

6. Conclusions

The scalar Young-parameter optimisation yields (15); it is the best algebraic value within the specified magnitude-bound estimate, not a system-wide optimal decay rate. This value is positive exactly when $\beta < 2\sqrt{ac}$. For $\beta > 0$, proportional feedback increases it toward a; the formal $\beta = 0$ extension is nondecreasing with finite saturation. Turning these algebraic facts into Mittag–Leffler stability statements still requires resolution of the operator-domain and comparison queries M01–M02. The delay calculation supplies a condition independent of the delay magnitude, not a delay-uniform decay rate. The disturbance comparison, if justified, implies an asymptotic residual radius rather than finite-time entry into its exact boundary. The supplied explicit-predictor computations are reproducible, but operator consistency and coupled equilibrium alignment remain M03–M04. These issues must be resolved before final publication approval. No patient data were used; prediction accuracy, clinical safety and artificial-pancreas performance are not established.

Supplementary Materials

The following supporting information can be downloaded at https://media.sciltp.com/articles/others/2609171635348181/ANDV-26070217-SI.zip: `simulate.py`, `test_scheme.py`, and a README describing dependencies, output locations and the unresolved model-consistency limitations.

Funding

This research received no external funding.

Institutional Review Board Statement

Not applicable.

Informed Consent Statement

Not applicable.

Data Availability Statement

No external data were used. The supplementary Python programs require NumPy and Matplotlib. The file `simulate.py` computes the figure trajectories and selected numerical metrics; the remaining entries of Tables 3 and 4 follow from the displayed algebraic formulas. The file `test_scheme.py`, which imports `simulate.py`, computes the endpoints and observed orders in Table 2. Reproduction of these recurrences does not verify their consistency with the stated ABC operator or the raw coupled model. Output-path details are given in the supplementary README.

Conflicts of Interest

The author declares no conflict of interest.

Use of AI and AI-Assisted Technologies

During proof review, OpenAI ChatGPT/Codex was used to assist with language editing, mathematical checks and reproducibility checks. After using this tool, the author reviewed and edited the content as needed and takes full responsibility for the content of the published article.

References

1. Bergman, R.N.; Phillips, L.S.; Cobelli, C. Physiologic evaluation of factors controlling glucose tolerance in man: Measurement of insulin sensitivity and beta-cell glucose sensitivity from the response to intravenous glucose. *J. Clin. Invest.* **1981**, *68*, 1456–1467. https://doi.org/10.1172/jci110398.
2. Ahmed, K.I.A.; Mirgani, S.M.; Seadawy, A.; et al. A comprehensive investigation of fractional glucose-insulin dynamics: Existence, stability, and numerical comparisons using residual power series and generalized Runge-Kutta methods. *J. Taibah Univ. Sci.* **2025**, *19*, 2460280. https://doi.org/10.1080/16583655.2025.2460280.
3. Alhazmi, M.; Mirgani, S.M.; Aljohani, A.F.; et al. Numerical simulation of a fractional glucose-insulin model via successive approximation and ABM schemes. *AIMS Math.* **2025**, *10*, 22817–22849. https://doi.org/10.3934/math.20251014.
4. Rafique, M.; Ur Rehamn, M.A.; Rafiq, M.; et al. Time delayed fractional diabetes mellitus model and consistent numerical algorithm. *Sci. Rep.* **2024**, *14*, 23871. https://doi.org/10.1038/s41598-024-74767-w.
5. AL-Mekhlafi, S.M.; Abou Hasan, M.M.; Al-Ali, H.A.; et al. A Crossover Optimal Control Framework for a Time-Delayed Fractional-Order Diabetes Model: Stability, Bifurcation, and Numerical Analysis. *Math. Methods Appl. Sci.* **2025**, *48*, 15723–15741. https://doi.org/10.1002/mma.70046.
6. Alhazmi, M.; Mirgani, S.M.; Saber, S. Hybrid Euler-Lagrange approach for fractional-order modeling of glucose-insulin dynamics. *Axioms* **2025**, *14*, 800. https://doi.org/10.3390/axioms14110800.
7. Saber, S.; Solouma, E. Advanced fractional modeling of diabetes: Bifurcation analysis, chaos control, and a comparative study of numerical methods Adams-Bashforth-Moulton and Laplace-Adomian-Padé method. *Indian J. Phys.* **2025**, *99*, 5151–5169. https://doi.org/10.1007/s12648-025-03712-y.
8. Saber, S.; Alahmari, A.; Shokeralla, A.A.; et al. Numerical Techniques for Solving Fractional Glucose-Insulin Regulatory Systems. *Lobachevskii J. Math.* **2025**, *46*, 5471–5483. https://doi.org/10.1134/s1995080225605405.
9. Saber, S.; Solouma, E.; Aljohani, A.F.; et al. A hybrid approach to diabetes modeling: Fractional derivatives and stochastic analysis. *AIMS Math.* **2026**, *11*, 5029–5061. https://doi.org/10.3934/math.2026206.
10. Shenbagam, M.; Kanagaraj, G.; Giri, J.; et al. Optimizing blood glucose regulation in type 1 diabetes: A fractional order controller approach. *AIP Adv.* **2024**, *14*, 045331. https://doi.org/10.1063/5.0199980.
11. Farman, M.; Hasan, A.; Xu, C.; et al. Computational techniques to monitoring fractional order type-1 diabetes mellitus model for feedback design of artificial pancreas. *Comput. Methods Programs Biomed.* **2024**, *257*, 108420. https://doi.org/10.1016/j.cmpb.2024.108420.
12. Atangana, A.; Baleanu, D. New fractional derivatives with nonlocal and non-singular kernel: Theory and application to heat transfer model. *Therm. Sci.* **2016**, *20*, 763–769. https://doi.org/10.2298/tsci160111018a.
13. Abdeljawad, T.; Baleanu, D. Discrete fractional differences with nonsingular discrete Mittag-Leffler kernels. *Adv. Differ. Equ.* **2016**, *2016*, 232. https://doi.org/10.1186/s13662-016-0949-5.
14. Abdeljawad, T. Different type kernel h-fractional differences and their fractional h-sums. *Chaos Solitons Fractals* **2018**, *116*, 146–156. https://doi.org/10.1016/j.chaos.2018.09.022.
15. Abdeljawad, T. On Riemann and Caputo fractional differences. *Comput. Math. Appl.* **2011**, *62*, 1602–1611. https://doi.org/10.1016/j.camwa.2011.03.036.
16. Syed Ali, M.; Narayanan, G.; Shekher, V.; et al. Global Mittag-Leffler stability analysis of impulsive fractional-order complex-valued BAM neural networks with time varying delays. *Commun. Nonlinear Sci. Numer. Simul.* **2020**, *83*, 105088. https://doi.org/10.1016/j.cnsns.2019.105088.
17. Narayanan, G.; Syed Ali, M.; Karthikeyan, R.; et al. Global Mittag-Leffler boundedness of nabla discrete-time fractional-order fuzzy complex-valued molecular models of mRNA and protein in regulatory mechanisms. *Commun. Nonlinear Sci. Numer. Simul.* **2024**, *129*, 107669. https://doi.org/10.1016/j.cnsns.2023.107669.
18. Kchaou, M.; Narayanan, G.; Syed Ali, M.; et al. Finite-time Mittag-Leffler synchronization of delayed fractional-order discrete-time complex-valued genetic regulatory networks: Decomposition and direct approaches. *Inf. Sci.* **2024**, *664*, 120337. https://doi.org/10.1016/j.ins.2024.120337.
19. Wei, Y.; Wei, Y.; Chen, Y.; et al. Mittag-Leffler stability of nabla discrete fractional-order dynamic systems. *Nonlinear Dyn.* **2020**, *101*, 407–417. https://doi.org/10.1007/s11071-020-05776-3.
20. Wei, Y.; Chen, Y.; Wei, Y.; et al. Lyapunov stability analysis for nonlinear nabla tempered fractional order systems. *Asian J. Control.* **2023**, *25*, 3057–3066. https://doi.org/10.1002/asjc.3003.
21. Wei, Y.; Zhao, L.; Wei, Y.; et al. Lyapunov theorem for stability analysis of nonlinear nabla fractional order systems. *Commun. Nonlinear Sci. Numer. Simul.* **2023**, *126*, 107443. https://doi.org/10.1016/j.cnsns.2023.107443.
22. Wu, X.; Yang, X.; Liu, D.Y.; et al. Wirtinger-based fractional summation inequality for stability analysis of nabla discrete fractional-order time-delay systems. *Nonlinear Dyn.* **2024**, *112*, 17055–17068. https://doi.org/10.1007/s11071-024-09916-x.

23. Mustapha, E.Z.; Abdellatif, E.O.; Karim, E.M.; et al. Fractional Caputo Operator and Takagi-Sugeno Fuzzy Modeling to Diabetes Analysis. *Symmetry* **2024**, *16*, 1395. https://doi.org/10.3390/sym16101395.
24. Narayanan, G.; Syed Ali, M.; Rajchakit, G.; et al. Stability analysis for nabla discrete fractional-order of Glucose-Insulin Regulatory System on diabetes mellitus with Mittag-Leffler kernel. *Biomed. Signal Process. Control.* **2023**, *80*, 104295. https://doi.org/10.1016/j.bspc.2022.104295.
25. Abdeljawad, T.; Al-Mdallal, Q.M. Discrete Mittag-Leffler kernel type fractional difference initial value problems and Gronwall's inequality. *J. Comput. Appl. Math.* **2018**, *339*, 218–230. https://doi.org/10.1016/j.cam.2017.10.021.
26. Chen, Y.; Li, X.; Liu, S. Finite-time stability of ABC type fractional delay difference equations. *Chaos Solitons Fractals* **2021**, *152*, 111430. https://doi.org/10.1016/j.chaos.2021.111430.